Catalysis Today 365 (2021) 172–180

Contents lists available at ScienceDirect

Catalysis Today

journal homepage: www.elsevier.com/locate/cattod

Determining the hydration energetics on carbon-supported Ru catalysts: An adsorption calorimetry and density functional theory study

Xianghui Zhang [a,b], Neeru Chaudhary [b], Megan R. Hawkins [a,e], Cody B. Cockreham [a,b,c], Chen Yang [a,b], Junnan Shangguan [d], Alyssa J.R. Hensley [b,d], Ya-Huei (Cathy) Chin [d], Su Ha [b], Jean-Sabin McEwen [b,e,f,g,h,*], Di Wu [a,b,e,i,*]

[a] Alexandra Navrotsky Institute for Experimental Thermodynamics, Washington State University, Pullman, WA, 99163, United States
[b] The Gene and Linda Voiland School of Chemical Engineering and Bioengineering, Washington State University, Pullman, WA, 99163, United States
[c] Earth and Environmental Sciences Division, Los Alamos National Laboratory, Los Alamos, NM 87545, United States
[d] Department of Chemical Engineering and Applied Chemistry, University of Toronto, Toronto M5S 3E5, Canada
[e] Department of Chemistry, Washington State University, Pullman, WA, 99164, United States
[f] Department of Physics and Astronomy, Washington State University, Pullman, WA, 99164, United States
[g] Department of Biological Systems Engineering, Washington State University, Pullman, WA, 99164, United States
[h] Institute for Integrated Catalysis, Pacific Northwest National Laboratory, Richland, WA 99352, United States
[i] Materials Science and Engineering, Washington State University, Pullman, WA, 99164, United States

ARTICLE INFO

Keywords:
Energetics
Hydrodeoxygenation
Catalyst characterization
Ruthenium supported on activated carbon
Density-functional theory
Calorimetry

ABSTRACT

Fundamental knowledge on the energetics at the interface between a water layer and a metal catalyst is essential so as to understand the roles that water can play in the synthesis, activation, and regeneration of noble metal-based catalysts. Here, we report the direct measurement of the enthalpy of water adsorption (Δh_{ads}) on activated carbon (C) and activated C-supported ruthenium (Ru) nanoparticles, which is a promising catalyst as applied to the hydrogenation/hydrodeoxygenation (HDO) of oxygenates (phenolics, aldehydes, *etc.*). Specifically, the near-zero coverage enthalpy of water adsorption on a C-supported Ru catalyst is -75.3 ± 0.4 kJ/(mol water), suggesting favorable water–metal binding. This is much more exothermic than that on C, which has an enthalpy of adsorption of -50.3 ± 1.3 kJ/(mol water). Despite the favorable initial binding, the magnitudes of enthalpies of water condensation on C and Ru-C indicate that overall, their surfaces are both hydrophobic. Moreover, the experimentally-measured near-zero coverage water adsorption enthalpy at the Ru sites is in very good agreement with our density functional theory based calculations. At low coverages, we obtain a water binding energy of −61.7 kJ/(mol water), which increases to −78.1 kJ/(mol water) at saturation. Complementary results are also obtained from a thermal analysis, which employed a thermogravimetric analysis–mass spectrometry (TG-MS), a spectroscopic investigation using *ex situ* diffuse reflectance infrared Fourier transform spectroscopy (DRIFTS), and a morphological evaluation with transmission electron microscopy (TEM). We point out that in carbon-supported metal catalysts, such as Ru-C, a strong hydration at near-zero coverage and relative weak water-surface interactions occur upon saturation. Such heterogeneity is essential and crucial for catalytic hydrogenation/HDO reactions that involve balanced interactions among the water-rich reactant mixture and nonpolar organic products.

1. Introduction

The energy crisis, global warming, and environmental pollution stimulate the development of alternative forms of energy from renewable sources such as sunlight, wind, hydropower, ocean, geothermal activities, hydrogen, and biomass [1–5]. Fuel production from biomass conversion into bio-oil followed by its catalytic upgrading dominates the renewable energy industry by ~70 % [6,7]. Among the various biomass conversion methods such as gasification and fermentation, fast pyrolysis is a cost-effective way of producing bio-oil [8]. Typically, the bio-oil

* Corresponding authors at: The Gene and Linda Voiland School of Chemical Engineering and Bioengineering, Washington State University, Pullman, WA, 99163, United States.
E-mail addresses: js.mcewen@wsu.edu (J.-S. McEwen), d.wu@wsu.edu (D. Wu).

https://doi.org/10.1016/j.cattod.2020.09.021
Received 15 June 2020; Received in revised form 17 September 2020; Accepted 30 September 2020
Available online 12 October 2020

obtained from biomass pyrolysis unavoidably contains a significant amount of highly oxygenated organic species, which not only exhibit a low heating value but also are corrosive and thermally unstable [9–11]. These compounds have made the direct pyrolysis products intrinsically incompatible with the current petroleum-derived oil. Thus, post pyrolysis deoxygenation (DO) is necessary to enhance the quality of bio-oil.

Two promising strategies for industrial-scale processes for upgrading bio-oil to engine fuels are catalytic cracking and hydrodeoxygenation (HDO) [12–14]. Upgrading with zeolite cracking, which mimics fluid catalytic cracking (FCC), does not work as expected due to its unsatisfactory performance. In comparison, HDO uses hydrogen as the reducing agent to hydrogenate and then cleave the carbon-oxygen bonds in the oxygenates, *via* chemistry similar to those of hydrodesulfurization (HDS), a mature industrial process that uses hydrogen to saturate heavy hydrocarbons and then cleave their carbon-sulfur bonds in heavy oil processing [12]. Typical HDO catalysts include sulfides [12,15] and supported transition or noble metal clusters/particles [16–20]. Ruthenium (Ru)-based catalysts [21–29] are a family of promising candidates owing to their high HDO performance and much lower cost as compared with other noble metal catalysts [30–34]. Taking advantage of the high surface area, mild acidity, and surface oxophilicity of activated carbon, catalysts with Ru nanoparticles supported on activated carbon (Ru-C) have been particularly attractive for catalytic HDO bio-oil upgrading [16,35].

Thus far, the synthesis of Ru-C catalysts, their structures and catalytic functions, and the resulting HDO reaction pathways have been extensively studied [21–29]. In particular, there have been several studies in the literature regarding the formation of water overlayers on Ru (0001) [36–41]. However, the hydration energetics of synthesized carbon-supported Ru catalysts has not been studied using integrated calorimetric methods and density functional theory (DFT) models. Yet, these energetic landscapes dictate the interactions of Ru and C with the reactants, intermediates, and transition states and in turn the HDO rates and selectivities. Fundamentally, water and Ru-C interactions are important because water is a major component of the reactant mixture. The starting bio-oil from fast pyrolysis contains about 15−30 wt% of water [42]. In addition, water is one of the products of an HDO reaction, which means subtle variations in the binding of water to a catalyst surface and local water concentration likely substantially impact the elementary steps and direction of surface reactions, the binding energetics of adsorbed species, including reactants, intermediates, and products. Water may also occupy and, in some cases, deactivate the catalytic sites once hydration is dominant on the catalyst surfaces due to surface flooding [43]. Moreover, the biphasic aqueous-oil system is one of the most promising reaction systems for bio-oil upgrading [44–46]. Finally, water can play multiple roles in a catalytic reaction itself, ranging from proton shuttling to forming hydroxyl groups that can act as Brønsted acid sites [47,48]. Therefore, it is essential to carry out fundamental studies on the hydration energetics of carbon-supported Ru catalysts.

Herein, we focus on the energetic landscape, as water molecules adsorb on and interact with Ru nanoparticles and with the C supports. Previously, the hydration energetics of nanoparticles, porous materials, and nuclear waste forms has been studied using adsorption calorimetry, in which the surface energetics were systematically probed as a function of water vapor partial pressure [49–55]. Here, we do not focus on the reaction engineering or the kinetics of HDO processes. To reveal the heterogeneity of Ru-C and its hydration energetics relavant to HDO, we carried out water adsorption calorimetry on activated carbon (C) and 1 wt% ruthenium supported on activated carbon (Ru-C), a representative carbon-based noble metal catalyst. Prior to calorimetric measurements, both samples were characterized using *ex situ* X-ray diffraction (XRD), *ex situ* diffuse reflectance infrared Fourier transform spectroscopy (DRIFTS), and transmission electron microscopy (TEM). Coupled with thermogravimetric analysis–mass spectrometry (TG-MS), we successfully monitored the dehydration processes for C and Ru-C. Further, the experimentally measured water adsorption enthalpy at near-zero coverage is compared to the coverage dependence of water adsorption as calculated from first principles using density functional theory (DFT), where the differential and the average binding energy values are obtained on Ru (0001). We also compare our results to those obtained on graphene and hydrogen-terminated graphene so as to obtain fundatmental insights into this complex adsorption system.

2. Experimental methods

2.1. Catalyst synthesis

Ru-C catalysts were synthesized with incipient wetness impregnation methods. Activated carbon powders were obtained from Norit (SX ULTRA CAT 8020-1, 1200 m^2/g, 1.4 cm^3/g pore volume, 90 % of particles <100 μm). The powders were treated at 2 °C/min to 300 °C and holding for 7 h in He (Linde certified standard, 99.999 %). After the heat treatment, Ru was introduced by incipient wetness impregnation using an aqueous $Ru(NO)(NO_3)_3$ solution, prepared by diluting the Ru precursor (Sigma Aldrich, CAS Number: 34513-98-9) in doubly-deionized water (>18 MΩ cm). The sample was then dried at 70 °C for 12 h under ambient condition, before treating under 5 % H_2/He (Linde certified standard) at 0.16 °C/s to 450 °C and maintaining at that temperature for 5 h. After the heat treatment, the sample was cooled to ambient temperature and then contacted with 5.5 % O_2/He (Linde certified standard) before exposure to the ambient air. The average Ru nanoparticle diameters were determined from volumetric hydrogen chemisorption at 40 °C.

2.2. Ex situ X-ray diffraction

Powder X-ray diffraction (XRD) patterns were collected at room temperature using a Rigaku Smartlab instrument (Cu *Kα*, 40 kV and 15 mA) from 20 to 80° at 2°/min for phase identification.

2.3. Transmission Electron Microscopy (TEM)

We examined the sample morphology using transmission electron microscopy (TEM, FEI Tecnai T20 with a LaB_6 cathode at 200 kV) in the Franceschi Microscopy and Imaging Center (FMIC) at Washington State University.

2.4. Ex situ diffuse reflectance infrared fourier transform spectroscopy (Ex situ DRIFTS)

The *ex situ* diffuse reflectance infrared Fourier transform spectroscopy (*ex situ* DRIFTS) measurements were carried out using a high-temperature cell (Spectra-Tech®) equipped with *ZnSe* windows. The background spectrum was collected over a pure diamond. The C and carbon-supported Ru samples were diluted using diamond before spectrum collection from 4000 to 650 cm^{-1}.

2.5. Thermal analysis

Thermal analysis was performed on a Netzsch Instrument STA 449 F3 coupled with mass spectrometry (Jupiter® STA-QMS 403 D Aëolos® quadrupole mass spectrometer) to determine the temperature at which the adsorbed species are removed from the material surface. About 15 mg of sample was placed in an alumina crucible and heated under nitrogen flow (50 mL/min) from 35 to 800 ℃ at 10 ℃/min. The exhaust species from the thermal analysis were introduced into the ionization chamber of the MS where they were ionized and fragmented by a cross beam electron impact ion source. The *m/z* ratios of the desorption product fragments were identified by an SEM detector with discrete dynodes and integrated Faraday cup. During thermal analysis, the adsorbed species on the C and carbon-supported Ru (Ru-C) samples were

determined qualitatively by the MS peaks. The desorption temperature for each sample was determined by this set of integrated TG-MS data.

2.6. Water adsorption calorimetry

Both C and Ru-C samples were pretreated at 150℃ in a vacuum oven for 24 h prior to the water adsorption calorimetry. The enthalpies of water adsorption for C and the carbon-supported Ru samples were determined using a modified Micromeritics 3Flex multiport adsorption analyzer in conjunction with a Setaram Sensys Evo microcalorimeter. This methodology allows for simultaneous measurements of the adsorption isotherm and the heat effect associated with each adsorption equilibrium at a particular temperature [52,56–58]. The sample (~60 mg) was placed in one side of a silica glass forked tube. The other side was left empty to function as a reference. The forked tube was inserted in the twin chambers of the microcalorimeter and connected to the analysis port of the adsorption analyzer. Each water vapor dose was ~ 0.2 μmol with an equilibrium time of 120 - 200 min and resulted in a calorimetric peak. The adsorption isotherm and associated energetic effects were recorded simultaneously. We derive the differential enthalpies of adsorption, kJ/(mol adsorbate), by dividing the total heat effect (kJ) with its corresponding uptake (mole of adsorbate). Calisto Processing software (AKTS, Switzerland) was employed for peak area calculation and data interpretation.

2.7. Density functional theory (DFT)

Theoretical investigations were performed to further understand the energetics of water adsorption on Ru and C. Ru was modeled with a Ru (0001) surface with dimensions of 9.4 × 9.4 × 21.5 Å with a $p\left(2\sqrt{3} \times 2\sqrt{3}\right)R30^{\circ}$ supercell. A single pristine graphene sheet was also modeled within a 14.8 × 14.8 × 20.0 Å unit cell. Finally, a graphene nanoribbon with hydrogen-terminated edges was modeled in a 17 × 29 × 21 Å unit cell. The calculations were carried out in spin restricted fashion in all three models. *Ab-initio* simulations were performed using the Vienna Ab initio Simulation Package (VASP) [59,60]. The core electrons were modeled using generalized gradient approximation (GGA) with the projector-augmented waves (PAW) method [61]. The pseudopotential for Ru, C, H, and O were the POTCARs released in Feb 2005, Apr 2002, Jun 2001, and Apr 2002, respectively. The optB88-vdW [62,63] exchange–correlation functional, which includes van der Waal contributions, was used in our DFT-based model.

In addition, we have compared our optB88-vdW functional results to those as obtained with the RPBE functional [64] using an adaptive weighted sum of their respective adsorption energies [65]. This method indicates that optB88-vdW would be the functional of choice for water adsorption on a pristine and a hydrogen-terminated graphene sheet as well as for Ru (0001), as was noted in the literature [66]. Water is also found to adsorb more strongly when using the optB88-vdW functional as compared to the RPBE functional (see Section 1 of the SI), which agrees better with our experimental data. Therefore, we used optB88-vdW functional for all our calculations as reported in the paper.

A plane wave basis set was expanded to a kinetic energy cutoff of 450 eV. Ground-state optimizations were performed using the conjugate gradient algorithm with electronic energies tolerance to 10^{-4} eV and forces on each atom were less than 0.03 eV/Å. Gaussian smearing (N = 0) [67,68] was applied for the pristine and H-edged graphene sheet, whereas the Methfessel–Paxton [69] smearing (N = 1) method was used for Ru slab to set partial occupancies of bands along with smearing width of 0.1 eV. Calculations for the water molecule in the gas phase were performed using a 14 × 15 × 16 Å box on a single Gamma **k**-point to span the Brillouin zone. The lattice constant optimized for graphene using the optB88-vdW and RPBE functionals were respectively 2.465 Å and 2.479 Å, which is consistent with our previous results where the PBE functional was used [70]. As for our modeling studies on Ru (0001), we obtained a value of $a = 2.717$ and $c = 4.284$ Å for the optimized lattice constants when using the optB88-vdW functional when using a (20 × 20 × 20) Gamma point centered **k**-point mesh, which is consistent with previous results [71–74]. The Ru (0001) surfaces were modeled using four atomic layers with a vacuum spacing of 15 Å, where the bottom two layers of the surfaces are fixed at their builk value positions, while the top two layers were allowed to relax. A (1 × 1 × 1) Monkhorst-Pack grid [75] was used to model the pristine graphene sheet, a (1 × 1 × 1) Monkhorst-Pack grid was used to model the hydrogen-terminated graphene nanoribbon, and a (3 × 3 × 1) Monkhorst-Pack grid was used to model the Ru (0001) surface.

Ab-initio MD (AIMD) simulations were performed to find the global minimum of a water molecule adsorbed on a given surface by carrying out simulated annealing with a time step of 2 fs. The hydrogen mass was set at 2 au to allow a larger time step in the AIMD simulations [47]. First, the surface with 1 H_2O molecule was placed in a random position and optimized using a DFT-based calculation. Then the system was annealed from 300 to 50 K for 10 ps, followed by second annealing from 50 to 20 K for another 10 ps. The system is then optimized in its ground state geometry. AIMD simulations were run using a single Gamma **k**-point and RMM-DIIS (ALGO = Very Fast) algorithm.

The coverage of water, Θ, is defined as the number of water molecules adsorbed per number of surface atoms in a unit cell and is expressed in monolayers (ML). The average adsorption energy, ($E_{ads}^{average}$), on a per molecule basis (kJ/(mol water), is defined as:

$$E_{ads}^{average} = \left(E_{total} - nE_{water} - E_{surface}\right)/n \quad (1)$$

where E_{total}, $E_{surface}$, and E_{water} represent the total energy of the system (surface with adsorbates present), the total energy of the clean surface (Ru or graphene or H-edge graphene sheet), and the total energy of an isolated water molecule in the gas phase, respectively. Also, n is the number of water molecules adsorbed on the surface. The differential adsorption energy, ($E_{ads}^{differential}$, kJ/(mol water)), is defined as:

$$E_{ads}^{differential} = \left(E_{ntotal} - E_{(n-1)total} - E_{water}\right) \quad (2)$$

A differential charge analysis was performed to obtain $\Delta\rho(\vec{r})$ which is the net electronic exchange upon adsorption of water on the surface. The value of $\Delta\rho(\vec{r})$ was calculated using the equation below:

$$\Delta\rho = \rho_{total} - \rho_{water} - \rho_{surface} \quad (3)$$

where $\rho_{total}(\vec{r})$, $\rho_{surface}(\vec{r})$, and $\rho_{water}(\vec{r})$represent the charge distribution for the adsorbed system (surface with adsorbates present), the clean surface (Ru or graphene or H-edged graphene sheet), and the water molecule in the gas phase, respectively.

The electronic interactions between water and the surface of the catalyst are further quantified using Eq. 4, where we integrated the absolute value of the differential charge density over the entire unit cell. This will give us a mean absolute charge transferred between the adsorbate and surface (Q) as calculated below: [76]

$$Q = 1/2 \int d\vec{r}\, |(\Delta\rho(\vec{r})| \quad (4)$$

where $\Delta\rho(\vec{r})$ is the differential charge density of the system.

3. Results and discussion

The weak XRD peak at ~ 42° belongs to Ru nanoparticles. (see Fig. 1**a**). *Ex Situ* DRIFTS in Fig. 1**b** suggests a very low degree of hydration with minimal presence of surface hydroxyl groups. In addition, there appears to be no detectable spectroscopic difference after the loading of 1 wt% Ru on the activated carbon. No peak is observed between 4000 and 3000 cm^{-1}, which is evidence of a very low degree of hydration on both samples. The peaks below 2000 cm^{-1} are tightly

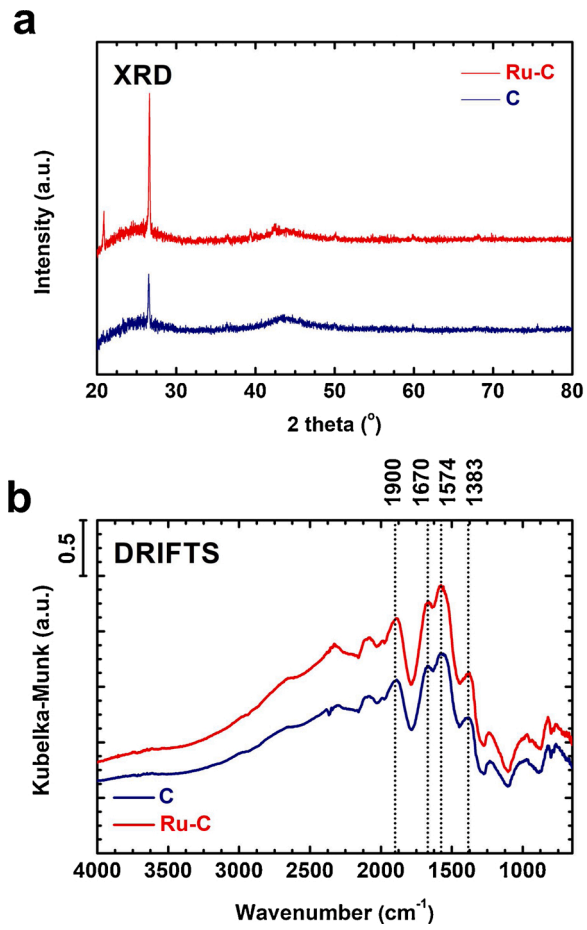

Fig. 1. Room temperature **(a)** *ex situ* XRD patterns and **(b)** *ex situ* DRIFTS spectra of activated carbon (C, navy) and Ru-doped activated carbon (Ru-C, red) (For interpretation of the references to colour in this figure legend, the reader is referred to the web version of this article).

correlated to the surface functional groups. Specifically, the peaks at about 1900 and 1670 cm^{-1} are attributed to the stretching vibration of C═O functional group. The feature at about 1574 cm^{-1} belongs to ν(C═C) vibration of the sp^2 rings, while the features around 1383 cm^{-1} are assigned to the aliphatic C—C bonds and/or carboxylate groups. DRIFTS was not able to directly identify the Ru species on the carbon surface [20].

The morphologies of the C and Ru-C samples were characterized by TEM. Fig. 2**a** shows the typical morphology of uniform activated carbon. There is no detectable large Ru particle in Fig. 2b, which is indeed an indication of nanosized Ru particles on the surface of activated carbon. Volumetric hydrogen chemisorption at 40 °C gives the average Ru nanoparticle diameter of 14 nm. Jin et al. and Sun et al. both found that once supported on activated carbon, Ru particles are much better dispersed as compared with Au, Pt, Fe, and Pd [20,77]. This phenomenon may originate from the existence of a significant amount of non-crystallized $[Ru(O)^x]^{\delta+}$ species on the carbon surface [78].

TG profiles of both samples, obtained during heating under flowing N_2, show very little weight loss, suggesting a low degree of hydration between 25 and 200 °C (see Fig. 3**a**) [79]. Fig. 3**b** shows the corresponding $m/z = 18$ signals from the MS during the temperature-programmed heating of the two samples. On Ru-C, the peak of $m/z = 18$ was observed from 100 to 150 ℃, which presents clear evidence of dehydration, where the water was removed and detected in the effluent stream. For the contrasting case of the C support without Ru, the lack of this water desorption feature in this temperature range suggests that dehydration does not occur to a significant extent (see Fig. 3**b**). Moreover, the thermal analysis results confirm that, after pretreatment and *in situ* degas at 150 ℃, the sample surfaces are fully dehydrated.

The water adsorption isotherms and corresponding differential enthalpies (Δh_{ads}), chemical potential ($\Delta \mu_{ads}$), and differential entropies (Δs_{ads}) for both samples are plotted in Fig. 4. The water adsorption isotherms of C and Ru-C appear to be hybrids of different *Types* according to the IUPAC classification (Fig. 4**a**). Specifically, at very low partial pressure (P/P_o, where P_o equals 23.77 mmHg at 25 °C [80]) or near-zero coverage, the isotherms of both C and Ru-C features relatively steep slopes, as seen in the low P/P_o range of *Type I & II* isotherms, which suggest favorable water-surface binding at near-zero coverage values. The remaining portions of the isotherms mimic the trend of *Type III* isotherms until saturation and indicate energetically unfavorable water-surface interactions followed by water-water intermolecular interactions (clustering at condensation). Hence, the hybrid nature of water adsorption isotherms is clear evidence of surface heterogeneity or hydrophobicity, as was observed on hydroxylated silica glass [52]. Interestingly, in earlier water adsorption calorimetry studies of microwave-synthesized carbon nanotube/graphene composites, the isotherms are all *Type II*, suggesting much more favorable surface hydration from near-zero coverage to condensation [79].

The near-zero differential enthalpies of water adsorption ($\Delta h_{ads\text{-}zero}$)

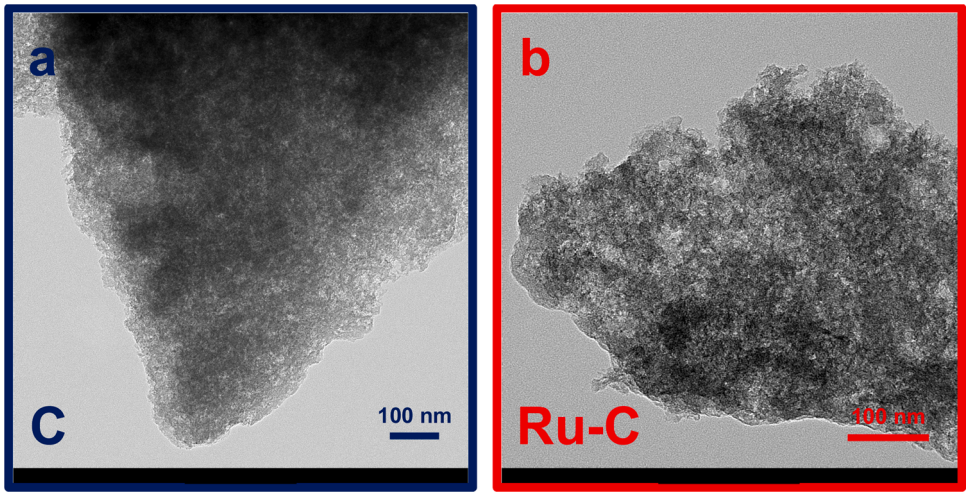

Fig. 2. TEM images of **(a)** activated carbon (C, navy) and **(b)** Ru-doped activated carbon (Ru-C, red) (For interpretation of the references to colour in this figure legend, the reader is referred to the web version of this article).

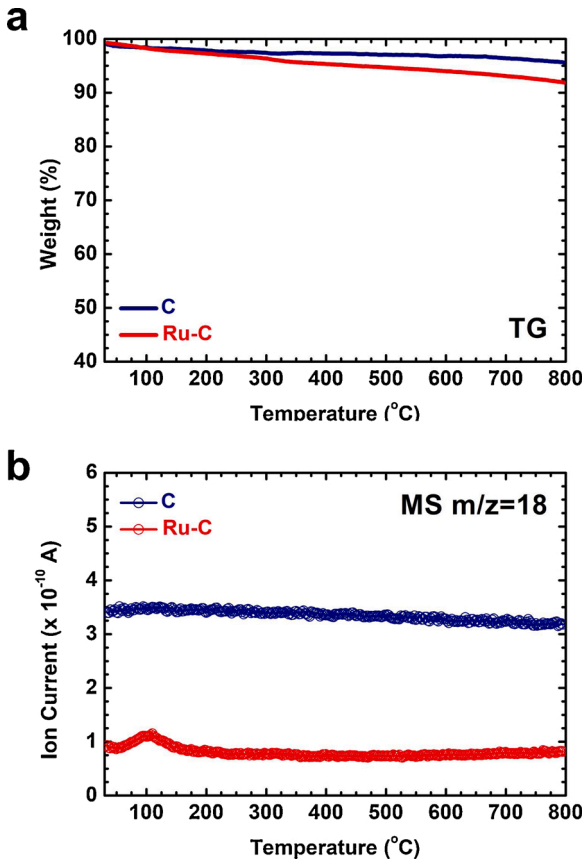

Fig. 3. **(a)** TG, and **(b)** MS profiles of activated carbon (C, navy) and carbon-supported Ru (Ru-C, red). The thermal analysis was performed from room temperature to 800 °C at 10 °C/min under flowing nitrogen (For interpretation of the references to colour in this figure legend, the reader is referred to the web version of this article).

are -50.3 ± 1.3 kJ/(mol water) for C and -75.3 ± 0.4 kJ/(mol water) for Ru-C. These exothermic $\Delta h_{\text{ads-zero}}$ values are in good agreement with the slope trend of isotherms and suggest strong initial chemisorption on the energetically most favorable surface sites. For the C sample, the most exothermic adsorption at near-zero coverage likely takes place on the hydroxyl groups on the carbon surface. The initial binding on Ru-C is likely caused by strong coordination between the water molecules and the exposed Ru sites on the Ru clusters or nanoparticles. Subsequently, the Δh_{ads} of each sample tends to be gradually less exothermic until reaching the plateaus at -37.7 ± 0.7 kJ/(mol water) for C and -36.3 ± 0.8 kJ/(mol water) for Ru-C (see Fig. 4**b**), both of which are less negative than the water condensation enthalpy on hydrophilic surfaces, -44.0 kJ/(mol water). Thus, the differential enthalpy plateaus for both samples occur at roughly the same value indicating that the presence of Ru species (1 wt%) does not significantly modify the overall thermodynamic properties of the surface. Moreover, the roughly 25 kJ/(mol water) difference in $\Delta h_{\text{ads-zero}}$ highlights the energetic difference of water adsorption caused by the introduction of the Ru species.

Further, we derived the partial molar free energies (chemical potential, $\Delta\mu_{\text{ads}}$) and differential entropies (Δs_{ads}) as a function of loading for both samples. The $\Delta\mu_{\text{ads}}$ profiles were calculated using the equation $\Delta\mu_{\text{ads}}=RT\ln(P/P_o)$, in which T = 298 K. P/P_o is the partial pressure, and water vapor at 1 atm is selected as the standard state [79,81]. Generally, the $\Delta\mu_{\text{ads}}$ curves are both negative for C and Ru-C reflecting spontaneous adsorption. For each sample, the $\Delta\mu_{\text{ads}}$ tends to be less exothermic as P/P_o increases until leveling at approximately the same plateau at slightly below zero. Such $\Delta\mu_{\text{ads}}$ profiles suggest spontaneous hydration throughout the pressure range studied. As more water is adsorbed, the adsorption of water becomes less spontaneous. Additionally, as expected, the near-zero chemical potential $\Delta\mu_{\text{ads-zero}}$ for Ru-C is -24.2 ± 0.2 kJ/(mol water), which is more exothermic than that of the C sample (-23.0 ± 0.4 kJ/(mol water), Fig. 4**c**). On the other hand, the Δs_{ads} profiles were derived using the equation $\Delta\mu_{\text{ads}} = \Delta h_{\text{ads}} - T\Delta s_{\text{ads}}$, in which T = 298 K. The shared general trend for C and Ru-C is that the Δs_{ads} is less negative as more water molecules are deposited onto the surfaces, indicating decreased entropy change as the degree of hydration increases. Specifically, the activated carbon (C) sample shows less negative $\Delta s_{\text{ads-zero}}$ at near-zero coverage suggesting that the water is initially loosely bonded (physisorbed) while still being highly mobile on the carbon surface resulting in a surface higher in entropy than that with tightly bonded chemisorbed water (see Fig. 4**d**). The Ru-C sample, in contrast, exhibits much more negative $\Delta s_{\text{ads-zero}}$, as the compelling evidence that the water molecules are chemisorbed onto the ruthenium (Ru) sites, leading to the formation of more ordered surface assemblages of water [40]. More quantitatively, the near-zero differential enthalpy of water adsorption $\Delta s_{\text{ads-zero}}$ is -0.17 ± 0.02 kJ/(mol·K). Since the standard molar entropy of water vapor is ~ 0.19 kJ/(mol·K) at 25 °C, the calorimetrically derived $\Delta s_{\text{ads-zero}}$ value in this study indicates that the water molecules adsorbed on Ru particles nearly lose all translation and rotation. At high water coverages, the Δs_{ads} curve levels at a plateau of -0.12 ± 0.03 kJ/(mol·K), which is in agreement with the entropy change at 25 °C (−0.08 kJ/(mol·K)) calculated using the Campbell–-Sellers approach with the function $\Delta s_{\text{ads}}^{\circ} = (0.70^{*}s_{\text{water vapor}}^{\circ} - 3.3\text{R}) - s_{\text{water vapor}}^{\circ}$, in which R is the gas constant, and $s_{\text{ads}}^{\circ} = 0.70^{*}s_{\text{water vapor}}^{\circ} - 3.3\text{R}$ [82]. Thus, at high coverage water appears to be in 2D ideal gas form that contains significant translation and rotation contributions. In sum, the Δs_{ads} profiles indicate that the water on C and Ru-C surfaces are highly dynamic clusters, which are energetically off the bulk water seen in our water bottle or on hydrophilic surfaces [81].

We have further calculated the adsorption energy of water within our DFT-based model. Water adsorbs on Ru (0001) at its most favorable adsorption site where the oxygen atom is centered on a top site at a height of ~ 2.3 Å above the surface (see Fig. 5). Its adsorption geometry is consistent with previous results [39,74]. At a coverage of 0.08 ML of water, we find its adsorption energy to be −61.7 kJ/(mol water). When increasing the water coverage on Ru (0001) from 0.08 to 0.66 ML the adsorption of water strengthens from −61.7 kJ/(mol water) to −78.1 kJ/(mol water) (see Fig. 6, with the corresponding structures in Fig. S1). As such, there is H-bonding between the water molecules at higher coverages. Interestingly, our DFT-based adsorption energy at high coverages closely correlates with the experimentally measured value of -75.3 ± 0.4 kJ/(mol water). Water strongly adsorbs on Ru as compared to when it adsorbs on a pristine graphene sheet, where water adsorbs with one of its H atoms directed on the C that forms a 6-membered ring in the sheet as illustrated in Fig. 5. This was found to be consistent with the reported results in the literature [83,84]. The resulting adsorption energy at its most favorable adsorption site is −20.3 kJ/(mol water) suggesting that water is only physisorbed. Such a physisorption configuration is also consistent with the fact that the water molecule is further away from the surface with the oxygen being ~ 3.5 Å above the surface with the hydrogen of the water molecule pointing toward the surface. We have further compared the adsorption of water to the case when it binds to a H-edge graphene sheet, where several possible adsorption sites were tested, as discussed in the SI. Our calculations suggest that water adsorbs with both of its H atoms directed toward the surface and with the oxygen at a distance of ~ 3.8 Å relative to the sheet with a resulting adsorption energy of −13.8 kJ/(mol water) (see Fig. 5).

Such a lower adsorption energy is clearly reflected in the differential charge analysis that is depicted in Fig. 5**b**. This analysis shows that the oxygen atom gains charge in all three cases upon adsorption. Overall, the charge transfer between the water molecule and the surface was higher on Ru (0001) than on the pristine and the H-edged graphene sheet, indicating stronger bonding on the Ru surface as compared to the

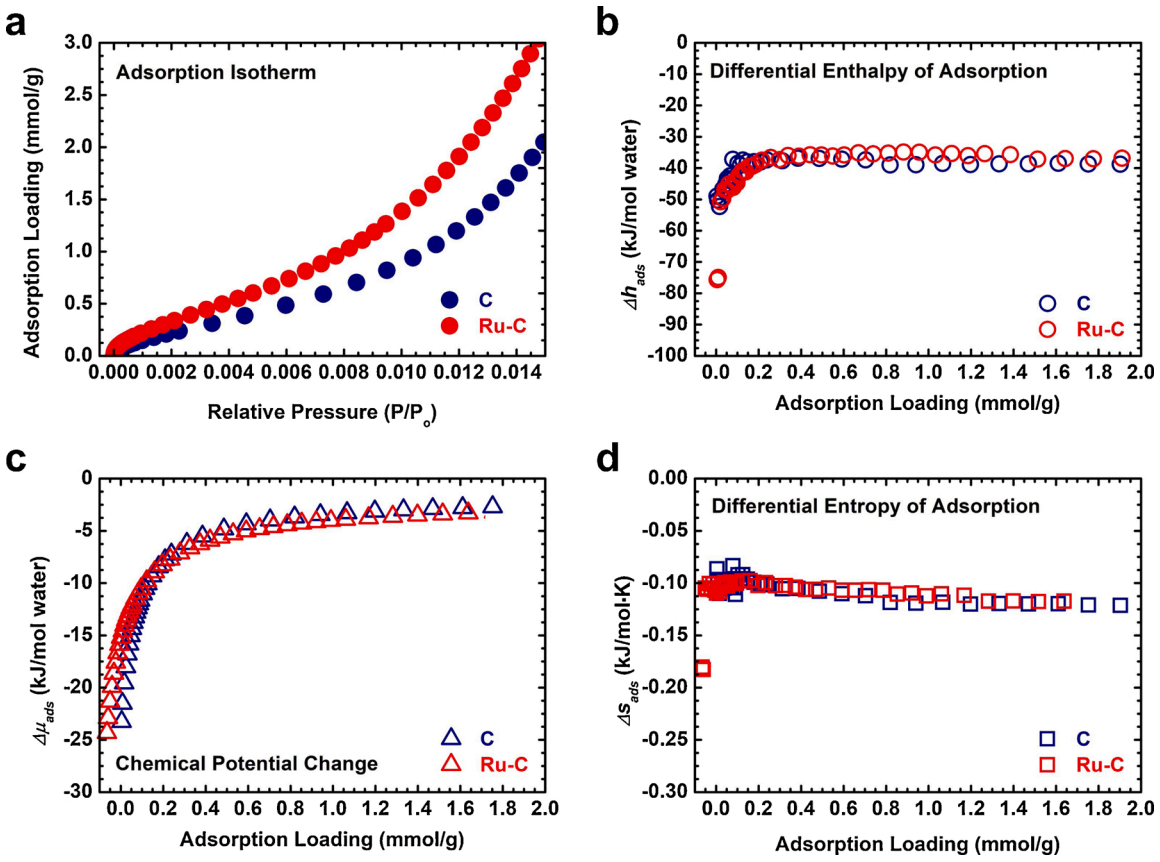

Fig. 4. (a) Water adsorption isotherms and corresponding (b) differential enthalpies, Δh_{ads}, (c) chemical potentials, $\Delta \mu_{ads}$, and (d) differential entropies, Δs_{ads}, of water adsorption curves at 25 °C on activated carbon (C) and carbon-supported Ru (Ru-C) samples.

graphene sheets, with mean charge transfer for Ru (0001), pristine graphene sheet, and H-edged graphene sheet being 0.49, 0.09 and 0.08 electrons respectively. As such, the low adsorption energy of water on the H-edge model of graphene and the pristine graphene sheet is directly correlated with the hydrophobicity of the activated carbon surface. On the other hand, when the activated carbon surface was modified with Ru, the interaction of water with the surface is favorably increased as compared to a H-edged graphene or a pristine graphene sheet on account of its higher adsorption energy.

Interestingly, our DFT-based results on the Ru (0001) surface (−61.7 kJ/(mol water)) and the H-edge graphene sheet (−20.3 kJ/(mol water)) at low coverages are both below those obtained from our calorimetry results, where heat of adsorption values of −75.3 ± 0.4 kJ/(mol water) were found at low coverage on the Ru-Ccatalyst while -36.3 ± 0.8 kJ/(mol water) was found on the saturated Ru-C catalyst sample. This gives an experimental heat of adsorption energy difference of 39.0 kJ/(mol water) while our DFT-based calculations give an adsorption energy difference of 41.4 kJ/(mol water), see Fig. 7. As such, even though it would seem that our DFT-based results systematically underestimate the adsorption strength of water for the adsorption of an isolated water molecule, it does seem to provide a more reasonable estimate of the adsorption energy when the surface is saturated with water with an average adsorption energy of −78.1 kJ/(mol water), see Fig. 6. These observations are also consistent with previous DFT-based calculations using the optB88-vdW functional as obtained in a recent benchmarking study on Pt (111) [65]. In that study, the experimental heat of adsorption value for water on Pt (111) was −51.0 kJ/mol, while the value obtained with the optB88-vdW functional was −39.0 kJ/(mol water) for an isolated water molecule on Pt (111). A similar value was also obtained for the optB86b-vdW functional where an adsorption energy value of −41.0 kJ/(mol water) is obtained. This suggests that the adsorbed water may be saturated locally in the experimental measurements, even if the coverage is low. We remark however that the optB88-vdW and optB86b-vdW functional values on Pt (111) are much closer to the experimental values as compared to the BEEF functional [65,85], where the adsorption energy value for water on Pt (111) is −21.0 kJ/(mol water). As such, van der Waals forces play a dominant role in the bonding of water to metal surfaces.

4. Conclusions

In this thermodynamic study, we integrated calorimetric measurements with DFT-based models to arrive at the following general conclusions of: (i) at near-zero coverage, the most exothermic enthalpies of water adsorption ($\Delta h_{ads\text{-}zero}$) are −75.3 ± 0.4 kJ/(mol water) for Ru-C, and −50.3 ± 1.3 kJ/(mol water) for activated C; (ii) By considering the particle size effects, higher surface energies in subnano or nanosized Ru particles than on single-crystal surfaces, and the recent optB88-vdW benchmarking results that are available in the literature, the calorimetric $\Delta h_{ads\text{-}zero}$ data is in very good agreement with the adsorption energy obtained using our DFT-based models, which ranges from Δh_{DFT} = −61.7 kJ/(mol water) for an isolated water molecule to −78.1 kJ/(mol water) at 0.66 ML; (iii) at intermediate coverages above 1 ML, both Δh_{ads} curves tend to be gradually less exothermic until saturation at about −37 kJ/(mol water). These plateaus indicate that water clustering occurs on a moderately hydrophobic activated carbon surface, and further suggest that the carbon-surface-confined water are highly dynamic clusters. Moreover, this set of data indicates that surface modification of carbon with noble metals, such as Ru, substantially enhances the water – catalyst affinity in the low coverage limit. Such

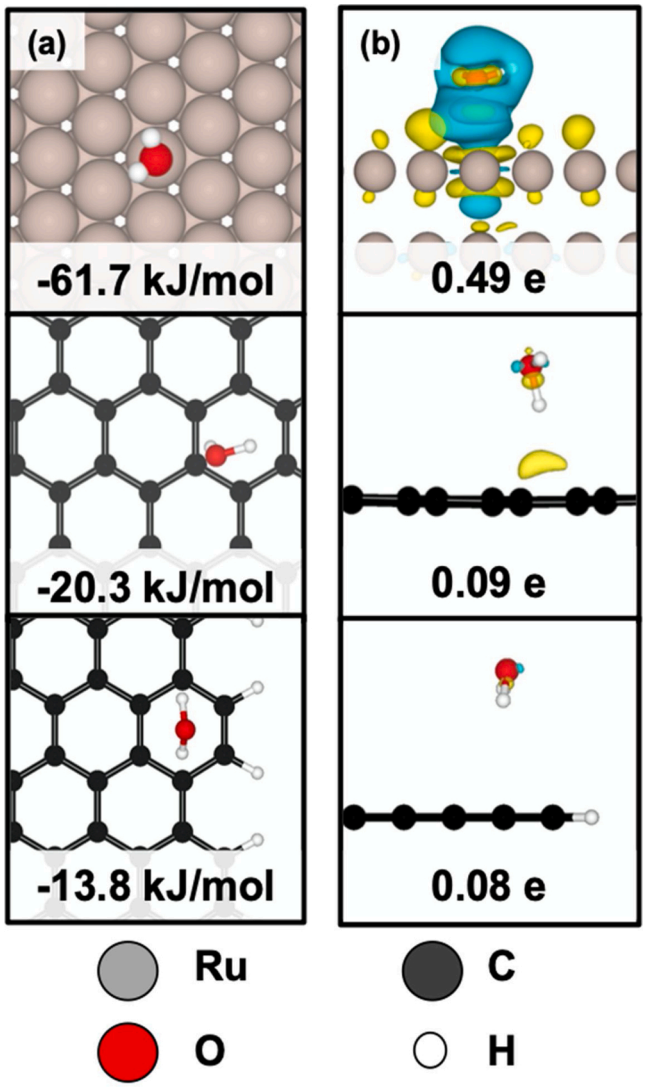

Fig. 5. Hydration energetics of Ru (0001) (top), pristine graphene sheet (middle), and H-edged graphene sheet (bottom) from DFT. **(a)** Top view, and **(b)** side view along with differential charge analysis at an isosurface of 0.0015 electrons/Bohr^3. Yellow: charge depletion; cyan: charge accumulation (For interpretation of the references to colour in this figure legend, the reader is referred to the web version of this article).

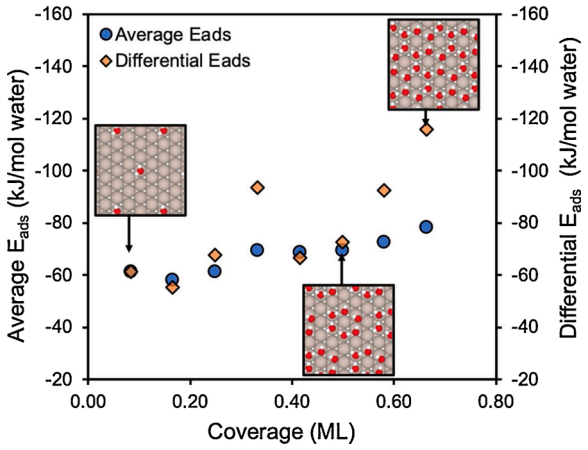

Fig. 6. Average and differential adsorption energies of water on Ru at various coverages. The grey, red and white spheres are Ru, O and H atoms, respectively (For interpretation of the references to colour in this figure legend, the reader is referred to the web version of this article).

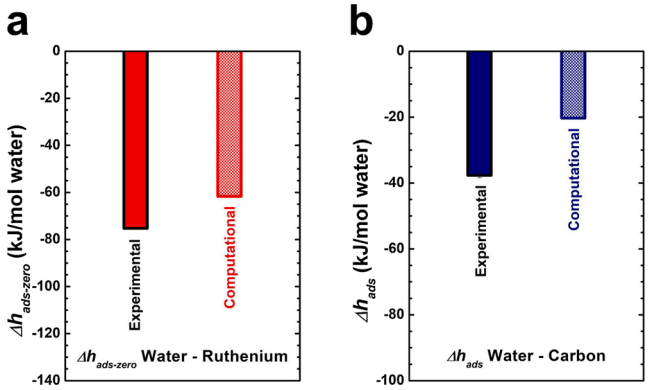

Fig. 7. Comparison of the energetics of **(a)** water – Ru, and **(b)** water – C interactions from adsorption calorimetry (experimental) and DFT (computational) studies.

heterogeneity is critical to enable effective HDO catalysis processes, in which complex organic fuels and water coexist. In the nearby future, we will report our study integrating CO adsorption calorimetry and DFT-based modeling to reveal the energetic distribution of Ru sites on the carbon surface as CO is supposed to selectively bind to metals while not binding to carbon.

CRediT authorship contribution statement

Xianghui Zhang: Validation, Software, Data curation. **Neeru Chaudhary:** Validation, Software, Data curation. **Megan R. Hawkins:** Validation. **Cody B. Cockreham:** Validation. **Chen Yang:** Validation. **Junnan Shangguan:** Writing - review & editing. **Alyssa J.R. Hensley:** Writing - review & editing. **Ya-Huei (Cathy) Chin:** Writing - review & editing. **Su Ha:** Writing - review & editing. **Jean-Sabin McEwen:** Conceptualization, Methodology, Software, Validation, Resources, Data curation, Writing - original draft, Writing - review & editing, Visualization, Supervision, Project administration, Funding acquisition. **Di Wu:** Conceptualization, Methodology, Software, Validation, Resources, Data curation, Writing - original draft, Writing - review & editing, Visualization, Supervision, Project administration, Funding acquisition.

Declaration of Competing Interest

The authors declare that they have no known competing financial interests or personal relationships that could have appeared to influence the work reported in this paper.

Acknowledgements

The work was primarily supported by the U.S. Department of Energy, Office of Science, Office of Basic Energy Sciences, Division of Chemical Sciences, Geosciences, and Biosciences within the Catalysis Science program, under award number DE-SC0014560. This work was, in part, supported by institutional funds from the Gene and Linda Voiland School of Chemical Engineering and Bioengineering and Alexandra Navrotsky Institute for Experimental Thermodynamics at Washington State University. This research used resources from the Center for Institutional Research Computing at Washington State University. Y.-H. C., A.J.R.H. and J.S. were supported by the Natural Sciences and Engineering Research Council of Canada (NSERC)'s Strategic Project Grant

(STPGP 493863-16) and Collaborative Research and Development Grants, DuPont, Ontario Centres of Excellence and the Canada Foundation for Innovation. A portion of the computer time for the computational work was performed using EMSL, a national scientific user facility sponsored by the Department of Energy's Office of Biological and Environmental Research and located at PNNL. This work was partially funded by the Joint Center for Deployment and Research in Earth Abundant Materials (JCDREAM) in Washington State. Xianghui Zhang is supported by Chambroad Distinguished Scholarship. Cody B. Cockreham received support from the Achievement Rewards for College Scientists (ARCS) Fellowship from the ARCS Seattle Chapter. PNNL is a multiprogram national laboratory operated for the US DOE by Battelle.

Appendix A. Supplementary data

Supplementary material related to this article can be found, in the online version, at https://doi.org/10.1016/j.cattod.2020.09.021.

References

[1] O. Ellabban, H. Abu-Rub, F. Blaabjerg, Renewable energy resources: current status, future prospects and their enabling technology, Renew. Sust. Energ. Rev. 39 (2014) 748–764, https://doi.org/10.1016/j.rser.2014.07.113.
[2] A. Demirbaş, Global renewable energy resources, Energy Sources 28 (2006) 779–792, https://doi.org/10.1080/00908310600718742.
[3] S. Bilgen, K. Kaygusuz, A. Sari, Renewable energy for a clean and sustainable future, Energy Sources 26 (2004) 1119–1129, https://doi.org/10.1080/00908310490441421.
[4] S.R. Bull, Renewable energy today and tomorrow, Proc. IEEE 89 (2001) 1216–1226, https://doi.org/10.1109/5.940290.
[5] N.L. Panwar, S.C. Kaushik, S. Kothari, Role of renewable energy sources in environmental protection: a review, Renew. Sustain. Energy Rev. 15 (2011) 1513–1524, https://doi.org/10.1016/j.rser.2010.11.037.
[6] X. Han, Y. Guo, X. Liu, Q. Xia, Y. Wang, Catalytic conversion of lignocellulosic biomass into hydrocarbons: a mini review, Catal. Today 319 (2019) 2–13, https://doi.org/10.1016/j.cattod.2018.05.013.
[7] W. Jin, L. Pastor-Pérez, D.K. Shen, A. Sepúlveda-Escribano, S. Gu, T. Ramirez Reina, Catalytic upgrading of biomass model compounds: novel approaches and lessons learnt from traditional hydrodeoxygenation – a review, ChemCatChem. 11 (2019) 924–960, https://doi.org/10.1002/cctc.201801722.
[8] S. Boonyasuwat, T. Omotoso, D.E. Resasco, S.P. Crossley, Conversion of guaiacol over supported Ru catalysts, Catal. Letters 143 (2013) 783–791, https://doi.org/10.1007/s10562-013-1033-3.
[9] A.N. Kay Lup, F. Abnisa, W.M.A.W. Daud, M.K. Aroua, A review on reaction mechanisms of metal-catalyzed deoxygenation process in bio-oil model compounds, Appl. Catal. A Gen. 541 (2017) 87–106, https://doi.org/10.1016/j.apcata.2017.05.002.
[10] S. Czernik, A.V. Bridgwater, Overview of applications of biomass fast pyrolysis oil, Energy Fuels 18 (2004) 590–598, https://doi.org/10.1021/ef034067u.
[11] D. Mohan, C.U. Pittman, P.H. Steele, Pyrolysis of wood/biomass for bio-oil: a critical review, Energy Fuels 20 (2006) 848–889, https://doi.org/10.1021/ef0502397.
[12] P.M. Mortensen, J.D. Grunwaldt, P.A. Jensen, K.G. Knudsen, A.D. Jensen, A review of catalytic upgrading of bio-oil to engine fuels, Appl. Catal. A Gen. 407 (2011) 1–19, https://doi.org/10.1016/j.apcata.2011.08.046.
[13] B. Valle, A. Remiro, N. García-Gómez, A.G. Gayubo, J. Bilbao, Recent research progress on bio-oil conversion into bio-fuels and raw chemicals: a review, J. Chem. Technol. Biotechnol. 94 (2019) 670–689, https://doi.org/10.1002/jctb.5758.
[14] A.V. Bridgwater, Production of high grade fuels and chemicals from catalytic pyrolysis of biomass, Catal. Today 29 (1996) 285–295, https://doi.org/10.1016/0920-5861(95)00294-4.
[15] D.C. Elliott, Historical developments in hydroprocessing bio-oils, Energy Fuels 21 (2007) 1792–1815, https://doi.org/10.1021/ef070044u.
[16] A.N. Kay Lup, F. Abnisa, W.M.A. Wan Daud, M.K. Aroua, A review on reactivity and stability of heterogeneous metal catalysts for deoxygenation of bio-oil model compounds, J. Ind. Eng. Chem. 56 (2017) 1–34, https://doi.org/10.1016/j.jiec.2017.06.049.
[17] Y. Jing, L. Dong, Y. Guo, X. Liu, Y. Wang, Chemicals from lignin: a review of catalytic conversion involving hydrogen, ChemSusChem 13 (2019), https://doi.org/10.1002/cssc.201903174.
[18] A. Bjelić, M. Grilc, M. Huš, B. Likozar, Hydrogenation and hydrodeoxygenation of aromatic lignin monomers over Cu/C, Ni/C, Pd/C, Pt/C, Rh/C and Ru/C catalysts: mechanisms, reaction micro-kinetic modelling and quantitative structure-activity relationships, Chem. Eng. J. 359 (2019) 305–320, https://doi.org/10.1016/j.cej.2018.11.107.
[19] J. Chang, T. Danuthai, S. Dewiyanti, C. Wang, A. Borgna, Hydrodeoxygenation of guaiacol over carbon-supported metal catalysts, ChemCatChem 5 (2013) 3041–3049, https://doi.org/10.1002/cctc.201300096.
[20] W. Jin, J.L. Santos, L. Pastor-Perez, S. Gu, M.A. Centeno, T.R. Reina, Noble metal supported on activated carbon for "Hydrogen free" HDO reactions: exploring economically advantageous routes for biomass valorisation, ChemCatChem. 11 (2019) 4434–4441, https://doi.org/10.1002/cctc.201900841.
[21] Y. Yang, Q. Liu, D. Li, J. Tan, Q. Zhang, C. Wang, L. Ma, Selective hydrodeoxygenation of 5-hydroxymethylfurfural to 2,5-dimethylfuran on Ru-MoO_x/C catalysts, RSC Adv. 7 (2017) 16311–16318, https://doi.org/10.1039/c7ra00605e.
[22] X. Zhang, W. Tang, Q. Zhang, Y. Li, L. Chen, Y. Xu, C. Wang, L. Ma, Production of hydrocarbon fuels from heavy fraction of bio-oil through hydrodeoxygenative upgrading with Ru-based catalyst, Fuel 215 (2018) 825–834, https://doi.org/10.1016/j.fuel.2017.11.111.
[23] Y. Weng, S. Qiu, C. Wang, L. Chen, Z. Yuan, M. Ding, Q. Zhang, L. Ma, T. Wang, Optimization of renewable C5 and C6 alkane production from acidic biomass hydrolysate over Ru/C catalyst, Fuel 170 (2016) 77–83, https://doi.org/10.1016/j.fuel.2015.12.007.
[24] P. Panagiotopoulou, D.G. Vlachos, Liquid phase catalytic transfer hydrogenation of furfural over a Ru/C catalyst, Appl. Catal. A Gen. 480 (2014) 17–24, https://doi.org/10.1016/j.apcata.2014.04.018.
[25] H. Wan, A. Vitter, R.V. Chaudhari, B. Subramaniam, Kinetic investigations of unusual solvent effects during Ru/C catalyzed hydrogenation of model oxygenates, J. Catal. 309 (2014) 174–184, https://doi.org/10.1016/j.jcat.2013.09.020.
[26] R.C. Nelson, B. Baek, P. Ruiz, B. Goundie, A. Brooks, M.C. Wheeler, B.G. Frederick, L.C. Grabow, R.N. Austin, Experimental and theoretical insights into the hydrogen-efficient direct hydrodeoxygenation mechanism of phenol over Ru/TiO_2, ACS Catal. 5 (2015) 6509–6523, https://doi.org/10.1021/acscatal.5b01554.
[27] C. Newman, X. Zhou, B. Goundie, I.T. Ghampson, R.A. Pollock, Z. Ross, M. C. Wheeler, R.W. Meulenberg, R.N. Austin, B.G. Frederick, Effects of support identity and metal dispersion in supported ruthenium hydrodeoxygenation catalysts, Appl. Catal. A Gen. 477 (2014) 64–74, https://doi.org/10.1016/j.apcata.2014.02.030.
[28] M. Rubeš, J. He, P. Nachtigall, O. Bludský, Direct hydrodeoxygenation of phenol over carbon-supported Ru catalysts: a computational study, J. Mol. Catal. A Chem. 423 (2016) 300–307, https://doi.org/10.1016/j.molcata.2016.07.007.
[29] A. Bjelić, M. Grilc, B. Likozar, Catalytic hydrogenation and hydrodeoxygenation of lignin-derived model compound eugenol over Ru/C: intrinsic microkinetics and transport phenomena, Chem. Eng. J. 333 (2018) 240–259, https://doi.org/10.1016/j.cej.2017.09.135.
[30] S. Arora, N. Gupta, V. Singh, Improved Pd/Ru metal supported graphene oxide nano-catalysts for hydrodeoxygenation (HDO) of vanillyl alcohol, vanillin and lignin, Green Chem. 22 (2020) 2018–2027, https://doi.org/10.1039/d0gc00052c.
[31] P.A. Lazaridis, S. Karakoulia, A. Delimitis, S.M. Coman, V.I. Parvulescu, K. S. Triantafyllidis, D-Glucose hydrogenation/hydrogenolysis reactions on noble metal (Ru, Pt)/activated carbon supported catalysts, Catal. Today 257 (2015) 281–290, https://doi.org/10.1016/j.cattod.2014.12.006.
[32] A. Sanna, T.P. Vispute, G.W. Huber, Hydrodeoxygenation of the aqueous fraction of bio-oil with Ru/C and Pt/C catalysts, Appl. Catal. B Environ. 165 (2015) 446–456, https://doi.org/10.1016/j.apcatb.2014.10.013.
[33] P.A. Lazaridis, S.A. Karakoulia, C. Teodorescu, N. Apostol, D. Macovei, A. Panteli, A. Delimitis, S.M. Coman, V.I. Parvulescu, K.S. Triantafyllidis, High hexitols selectivity in cellulose hydrolytic hydrogenation over platinum (Pt) vs. ruthenium (Ru) catalysts supported on micro/mesoporous carbon, Appl. Catal. B Environ. 214 (2017) 1–14, https://doi.org/10.1016/j.apcatb.2017.05.031.
[34] M. Kim, J.M. Ha, K.Y. Lee, J. Jae, Catalytic transfer hydrogenation/hydrogenolysis of guaiacol to cyclohexane over bimetallic RuRe/C catalysts, Catal. Commun. 86 (2016) 113–118, https://doi.org/10.1016/j.catcom.2016.08.022.
[35] M. Patel, A. Kumar, Production of renewable diesel through the hydroprocessing of lignocellulosic biomass-derived bio-oil: a review, Renew. Sust. Energ. Rev. 58 (2016) 1293–1307, https://doi.org/10.1016/j.rser.2015.12.146.
[36] M. Tatarkhanov, D.F. Ogletree, F. Rose, T. Mitsui, E. Fomin, S. Maier, M. Rose, J. I. Cerdá, M. Salmeron, Metal- and hydrogen-bonding competition during water adsorption on Pd(111) and Ru(0001), J. Am. Chem. Soc. 131 (2009) 18425–18434, https://doi.org/10.1021/ja907468m.
[37] P.J. Feibelman, Partial dissociation of water on Ru(0001), Science 295 (2002) 99–102, https://doi.org/10.1126/science.1065483.
[38] G. Materzanini, G.F. Tantardini, P.J.D. Lindan, P. Saalfrank, Water adsorption at metal surfaces: a first-principles study of the p(3×3) R30° H_2O bilayer on Ru (0001), Phys. Rev. B 71 (2005) 155414, https://doi.org/10.1103/PhysRevB.71.155414.
[39] A. Michaelides, A. Alavi, D.A. King, Different surface chemistries of water on Ru {0001}: from monomer adsorption to partially dissociated bilayers, J. Am. Chem. Soc. 125 (2003) 2746–2755, https://doi.org/10.1021/ja028855u.
[40] S. Haq, C. Clay, G.R. Darling, G. Zimbitas, A. Hodgson, Growth of intact water ice on Ru(0001) between 140 and 160 K: experiment and density-functional theory calculations, Phys. Rev. B 73 (2006) 115414, https://doi.org/10.1103/PhysRevB.73.115414.
[41] S. Schnur, A. Groß, Properties of metal-water interfaces studied from first principles, New J. Phys. 11 (2009) 125003, https://doi.org/10.1088/1367-2630/11/12/125003.
[42] Q. Bu, H. Lei, A.H. Zacher, L. Wang, S. Ren, J. Liang, Y. Wei, Y. Liu, J. Tang, Q. Zhang, R. Ruan, A review of catalytic hydrodeoxygenation of lignin-derived phenols from biomass pyrolysis, Bioresour. Technol. 124 (2012) 470–477, https://doi.org/10.1016/j.biortech.2012.08.089.
[43] P. Tereshchuk, J.L.F. Da Silva, Ethanol and water adsorption on close-packed 3d, 4d, and 5d transition-metal surfaces: a density functional theory investigation with van der Waals correction, J. Phys. Chem. C 116 (2012) 24695–24705, https://doi.org/10.1021/jp308870d.

[44] M.V. Vener, X. Rozanska, J. Sauer, Protonation of water clusters in the cavities of acidic zeolites: $(H_2O)_n$·H-chabazite, n = 1-4, Phys. Chem. Chem. Phys. 11 (2009) 1702–1712, https://doi.org/10.1039/b817905k.
[45] M.Y. Chen, Y.B. Huang, H. Pang, X.X. Liu, Y. Fu, Hydrodeoxygenation of lignin-derived phenols into alkanes over carbon nanotube supported Ru catalysts in biphasic systems, Green Chem. 17 (2015) 1710–1717, https://doi.org/10.1039/c4gc01992j.
[46] T. Wang, M.W. Nolte, B.H. Shanks, Catalytic dehydration of C6 carbohydrates for the production of hydroxymethylfurfural (HMF) as a versatile platform chemical, Green Chem. 16 (2014) 548–572, https://doi.org/10.1039/c3gc41365a.
[47] A.J.R. Hensley, Y. Wang, D. Mei, J.-S. McEwen, Mechanistic effects of water on the Fe-catalyzed hydrodeoxygenation of phenol the role of Brønsted acid sites, ACS Catal. 8 (2018) 2200–2208, https://doi.org/10.1021/acscatal.7b02576.
[48] Y. Yoon, R. Rousseau, R.S. Weber, D. Mei, J.A. Lercher, First-principles study of phenol hydrogenation on pt and ni catalysts in aqueous phase, J. Am. Chem. Soc. 136 (2014) 10287–10298, https://doi.org/10.1021/ja501592y.
[49] X. Zhang, C.B. Cockreham, Z. Huang, H. Sun, C. Yang, O.G. Marin-flores, B. Wang, X. Guo, S. Ha, H. Xu, D. Wu, Thermodynamics of water−cationic species−framework guest− host interactions within transition metal ion-exchanged mordenite relevant to selective anaerobic oxidation of methane to methanol, J. Phys. Chem. Lett. 11 (2020) 4774–4784, https://doi.org/10.1021/acs.jpclett.0c01331.
[50] S.V. Ushakov, A. Navrotsky, Direct measurements of water adsorption enthalpy on hafnia and zirconia, Appl. Phys. Lett. 87 (2005) 164103, https://doi.org/10.1063/1.2108113.
[51] D. Gouvêa, S.V. Ushakov, A. Navrotsky, Energetics of CO_2 and H_2O adsorption on zinc oxide, Langmuir 30 (2014) 9091–9097, https://doi.org/10.1021/la500743u.
[52] D. Wu, X. Guo, H. Sun, A. Navrotsky, Energy landscape of water and ethanol on silica surfaces, J. Phys. Chem. C 119 (2015) 15428–15433, https://doi.org/10.1021/acs.jpcc.5b04271.
[53] N. Birkner, A. Navrotsky, Rapidly reversible redox transformation in nanophase manganese oxides at room temperature triggered by changes in hydration, Proc. Natl. Acad. Sci. (**111**, 2014, 6209-6214), https://doi.org/10.1073/pnas.1320014111.
[54] X. Zhang, C.B. Cockreham, E. Yılmaz, G. Li, N. Li, S. Ha, L. Fu, J. Qi, H. Xu, D. Wu, Energetic cost for being “redox-site-rich” in pseudocapacitive energy storage with nickel-aluminum layered double hydroxide materials, J. Phys. Chem. Lett. 11 (2020) 3745–3753, https://doi.org/10.1021/acs.jpclett.0c00865.
[55] A.A. Levchenko, G. Li, J. Boerio-Goates, B.F. Woodfield, A. Navrotsky, TiO_2 stability landscape: polymorphism, surface energy, and bound water energetics, Chem. Mater. 18 (2006) 6324–6332, https://doi.org/10.1021/cm061183c.
[56] G. Li, H. Sun, H. Xu, X. Guo, D. Wu, Probing the energetics of molecule – material interactions at interfaces and in nanopores, J. Phys. Chem. C 121 (2017) 26141–26154, https://doi.org/10.1021/acs.jpcc.7b07450, acs.jpcc.7b07450.
[57] D. Wu, J.J. Gassensmith, D. Gouveîa, S. Ushakov, J.F. Stoddart, A. Navrotsky, Direct calorimetric measurement of enthalpy of adsorption of carbon dioxide on CD-MOF-2, a green metal-organic framework, J. Am. Chem. Soc. 135 (2013) 6790–6793, https://doi.org/10.1021/ja402315d.
[58] D. Wu, T.M. McDonald, Z. Quan, S.V. Ushakov, P. Zhang, J.R. Long, A. Navrotsky, Thermodynamic complexity of carbon capture in alkylamine-functionalized metal-organic frameworks, J. Mater. Chem. A 3 (2015) 4248–4254, https://doi.org/10.1039/c4ta06496h.
[59] G. Kresse, J. Hafner, Ab initio molecular dynamics for liquid metals, Phys. Rev. B 47 (1993) 558–561, https://doi.org/10.1103/PhysRevB.47.558.
[60] G. Kresse, J. Furthmüller, Efficient iterative schemes for ab initio total-energy calculations using a plane-wave basis set, Phys. Rev. B 54 (1996) 11169–11186, https://doi.org/10.1103/PhysRevB.54.11169.
[61] G. Kresse and D. Joubert, From ultrasoft pseudopotentials to the projector augmented-wave method, Phys. Rev. B 59 (1999) 1758–1775, https://doi.org/10.1103/PhysRevB.59.1758.
[62] J. Klime, D.R. Bowler, A. Michaelides, Van der Waals density functionals applied to solids, Phys. Rev. B 83 (2011) 1–13, https://doi.org/10.1103/PhysRevB.83.195131.
[63] J. Klimeš, D.R. Bowler, A. Michaelides, Chemical accuracy for the van der Waals density functional, J. Phys. Condens. Matter 22 (2010) 022201, https://doi.org/10.1088/0953-8984/22/2/022201.
[64] B. Hammer, L.B. Hansen, J.K. Nørskov, Improved adsorption energetics within density-functional theory using revised Perdew-Burke-Ernzerhof functionals, Phys. Rev. B 59 (1999) 7413–7421, https://doi.org/10.1103/PhysRevB.59.7413.
[65] A.J.R. Hensley, K. Ghale, C. Rieg, T. Dang, E. Anderst, F. Studt, C.T. Campbell, J. S. McEwen, Y. Xu, DFT-based method for more accurate adsorption energies: an adaptive sum of energies from RPBE and vdW density functionals, J. Phys. Chem. C 121 (2017) 4937–4945, https://doi.org/10.1021/acs.jpcc.6b10187.
[66] J. Carrasco, J. Klimeš, A. Michaelides, The role of van der Waals forces in water adsorption on metals, J. Chem. Phys. 138 (2013) 024708, https://doi.org/10.1063/1.4773901.
[67] C. Isvoranu, J. Åhlund, B. Wang, E. Ataman, N. Mårtensson, C. Puglia, J. N. Andersen, M.L. Bocquet, J. Schnadt, Electron spectroscopy study of the initial stages of iron phthalocyanine growth on highly oriented pyrolitic graphite, J. Chem. Phys. 131 (2009) 214709, https://doi.org/10.1063/1.3259699.
[68] I.C. Gerber, A.V. Krasheninnikov, A.S. Foster, R.M. Nieminen, A first-principles study on magnetic coupling between carbon adatoms on graphene, New J. Phys. 12 (2010) 113021, https://doi.org/10.1088/1367-2630/12/11/113021.
[69] M. Methfessel, A.T. Paxton, High-precision sampling for Brillouin-zone integration in metals, Phys. Rev. B 40 (1989) 3616–3621, https://doi.org/10.1103/PhysRevB.40.3616.
[70] G.G. Huang, Y.F. Liu, X.X. Wu, J.J. Cai, Activated carbons prepared by the KOH activation of a hydrochar from garlic peel and their CO_2 adsorption performance, New Carbon Mater. 34 (2019) 247–257, https://doi.org/10.1016/S1872-5805(19)60014-4.
[71] F. Mehmood, R. Pachter, W. Lu, J.J. Boeckl, Adsorption and diffusion of oxygen on single-layer graphene with topological defects, J. Phys. Chem. C 117 (2013) 10366–10374, https://doi.org/10.1021/jp312159v.
[72] A. Pulido, M. Boronat, A. Corma, Theoretical investigation of gold clusters supported on graphene sheets, New J. Chem. 35 (2011) 2153–2161, https://doi.org/10.1039/c1nj20215d.
[73] Z. Hou, X. Wang, T. Ikeda, K. Terakura, M. Oshima, M.A. Kakimoto, S. Miyata, Interplay between nitrogen dopants and native point defects in graphene, Phys. Rev. B 85 (2012) 165439, https://doi.org/10.1103/PhysRevB.85.165439.
[74] S. Meng, E.G. Wang, S. Gao, Water adsorption on metal surfaces: a general picture from density functional theory studies, Phys. Rev. B 69 (2004) 195404, https://doi.org/10.1103/PhysRevB.69.195404.
[75] J.D. Pack, H.J. Monkhorst, “Special points for Brillouin-zone integrations”-a reply, Phys. Rev. B 16 (1977) 1748, https://doi.org/10.1103/PhysRevB.16.1748.
[76] L.M. Ghiringhelli, R. Caputo, L.D. Site, Phenol near Ni(111), Ni(110), and Ni(221) surfaces in a vertical ring geometry: a density functional study of the oxygen-surface bonding and O—H cleavage, Phys. Rev. B 75 (2007) 113403, https://doi.org/10.1103/PhysRevB.75.113403.
[77] J. Sun, A.M. Karim, H. Zhang, L. Kovarik, X. Shari, A.J. Hensley, J. McEwen, Y. Wang, Carbon-supported bimetallic Pd – Fe catalysts for vapor-phase hydrodeoxygenation of guaiacol, J. Catal. 306 (2013) 47–57, https://doi.org/10.1016/j.jcat.2013.05.020.
[78] P.A. Lazaridis, S. Karakoulia, A. Delimitis, S.M. Coman, V.I. Parvulescu, K. S. Triantafyllidis, D -Glucose hydrogenation/hydrogenolysis reactions on noble metal (Ru, Pt)/activated carbon supported catalysts, Catal. Today 257 (2015) 281–290, https://doi.org/10.1016/j.cattod.2014.12.006.
[79] G. Li, S. Sarwar, X. Zhang, C. Yang, X. Guo, X. Zhang, D. Wu, Surface energetics of carbon nanotubes-based nanocomposites fabricated by microwave-assisted approach, J. Mater. Res. 34 (2019) 3361–3367, https://doi.org/10.1557/jmr.2019.222.
[80] D. Wu, A. Navrotsky, Probing the energetics of organic-nanoparticle interactions of ethanol on calcite, Proc. Natl. Acad. Sci. 112 (2015) 5314–5318, https://doi.org/10.1073/pnas.1505874112.
[81] J. Wang, E. Yllmaz, X. Zhang, H. Li, R. Zhang, X. Guo, H. Sun, B. Wang, D. Wu, Hydration energetics of a diamine-appended metal-organic framework carbon capture sorbent, J. Phys. Chem. C 124 (2019) 398–403, https://doi.org/10.1021/acs.jpcc.9b08008.
[82] C.T. Campbell, J.R.V. Sellers, The entropies of adsorbed molecules, J. Am. Chem. Soc. 134 (2012) 18109–18115, https://doi.org/10.1021/ja3080117.
[83] J. Ma, A. Michaelides, D. Alfè, L. Schimka, G. Kresse, E. Wang, Adsorption and diffusion of water on graphene from first principles, Phys. Rev. B 84 (2011) 033402, https://doi.org/10.1103/PhysRevB.84.033402.
[84] L. Jiang, J. Wang, P. Liu, W. Song, B. He, Study of water adsorption on graphene edges, RSC Adv. 8 (2018) 11216–11221, https://doi.org/10.1039/c8ra00002f.
[85] J. Wellendorff, T.L. Silbaugh, D. Garcia-Pintos, J.K. Nørskov, T. Bligaard, F. Studt, C.T. Campbell, A benchmark database for adsorption bond energies to transition metal surfaces and comparison to selected DFT functionals, Surf. Sci. 640 (2015) 36–44, https://doi.org/10.1016/j.susc.2015.03.023.